RESEARCH ARTICLE

Turning the Tap: Conformational Control of Quantum Interference to Modulate Single Molecule Conductance

Feng Jiang, Douglas I. Trupp, Norah Algethami, Haining Zheng, Wenxiang He, Afaf Alqorashi, Chenxu Zhu, Chun Tang, Ruihao Li, Junyang Liu, Hatef Sadeghi, Jia Shi, Ross Davidson, Marcus Korb, Alexandre N. Sobolev, Masnun Naher, Sara Sangtarash,* Paul J. Low,* Wenjing Hong,* Colin J. Lambert*

Abstract: Together with the more intuitive and commonly recognized conductance mechanisms of charge-hopping and tunneling, quantum interference (QI) phenomena have been identified as important factors affecting charge transport through molecules. Consequently, establishing simple, flexible molecular design strategies to understand, control and exploit QI in molecular junctions poses an exciting challenge. Here we demonstrate that destructive quantum interference (DQI) in meta-substituted phenylene ethylene-type oligomers (m-OPE) can be tuned by changing the position and conformation of pendant methoxy (OMe) substituents around the central phenylene ring. These substituents play the role of molecular-scale 'taps', which can be switched on or off to control the current flow through a molecule. Our experimental results conclusively verify recently postulated magic ratio and orbital product rules, and highlight a novel chemical design strategy for tuning and gating DQI features, to create single-molecule devices with desirable electronic functions.

Introduction

Measurements of the conductance of electrode | molecule | electrode junctions, interpreted with the aid of theoretical treatments and computational modelling, have given insight into the fundamentals of through-molecule electron transport, leading to the design of molecular wires,[1] molecular switches[2] and molecular diodes[3]. One of the most interesting aspects of single-molecule electronics to emerge from these studies is the phenomena of room-temperature quantum interference (QI).[4] This concept was first introduced in 1909 to prove the wave characteristics of photons in the double-slit experiments.[5] Now it is widely investigated in diverse research areas, such as nanophotonics,[6] superconductivity[7] and quantum metrology.[8] In the studies of molecular junctions, QI arises when the de Broglie waves of electrons progressing from one electrode to the other pass through different energetically accessible pathways across the molecule junction, causing interference patterns within the molecule.[9] Constructive QI (CQI) occurs when the interference pattern has a large amplitude at the point of molecular contact to both the source and drain electrodes, causing high through-molecule conductance. Conversely, destructive QI (DQI) results in low amplitude of the propagating electron wave at one or both of the electrode-molecule contacts, causing extremely low through-molecule conductance.[10] The ability to convert between these two scenarios by tuning the molecular pathways can offer an exciting range of opportunities to regulate charge transport through molecules, without changing molecular backbone structure, length or redox state.

Recently a number of studies have contributed to the identification of mechanisms for conductance tuning of single-molecule junctions using QI phenomena, including the impact of anchor groups,[11] the position of heteroatoms within the molecular backbone[12] and bridge modification.[13] Following theoretical predictions of DQI due to pendant oxygen and bipyridene groups attached to conjugated molecular cores [T.A. Papadopoulos, I.M. Grace and CJL, Phys. Rev. B74 193306, (2006); C. M. Finch, V. M. García-Suárez, and CJL, Phys. Rev. B79, 033405 (2009)], and subsequent experimental confirmation [T. Wandlowski, W. Hong, A. Mishchenko, P. Moreno-Garcia, H. Valkenier, J. C. Hummellen, A. Putz, G. Meszaros, D. Z. Manrique and CJ Lambert, Beilstein J. Nanotechnology 2 699 (2011); V. Kaliginedi, P. Moreno-Garcia, H. Valkenier, WJ Hong, V.M. Garcia-Suarez, P. Buiter, J.L.H. Otten, J.C. Hummelen, C.J. Lambert and T. Wandlowski, J. Am. Chem. Soc. 134 5262-5275 (2012)], a study of QI effects in molecular junctions of π-conjugated systems was carried out by Guédon et al. using the conducting atomic force microscopy technique.[14] Arroyo et al. studied QI effects in a central phenyl ring by varying the coupling to a variety of anchor groups.[15] Manrique et al. also tuned the QI effects through heteroatom substitution and proposed a quantum circuit rule for designing molecular devices and materials.[16] Furthermore, the experimental and theoretical breakthroughs realized by Garner et al. demonstrated that destructive QI effects could also be achieved in silicon-based σ-orbital systems.[4a] More recently, Li et al. and Bai et al. observed an anti-resonance feature and tuned the destructive QI through electrochemical gating.[17] Although state-of-art theoretical studies have been devoted to the

[*] Feng Jiang, Haining Zheng, Wenxiang He, Chenxu Zhu, Chun Tang, Ruihao Li, Dr. Junyang Liu, Prof. Jia Shi, Prof. Wenjing Hong
State Key Laboratory of Physical Chemistry of Solid Surfaces
College of Chemistry and Chemical Engineering, iChEM
Xiamen University, Xiamen 361005 (China)
E-mail: whong@xmu.edu.cn
Douglas I. Trupp, Marcus Korb, Alexandre N. Sobolev, Masnun Naher, Prof. Paul J. Low
School of Molecular Sciences, University of Western Australia, 35 Stirling Highway, Crawley, Western Australia, 6009, Australia
E-mail: paul.low@uwa.edu.au
Norah Algethami, Dr. Afaf Alqorashi, Dr. Hatef Sadeghi, Dr. Sara Sangtarash, Prof. Colin J. Lambert
Department of Physics, Lancaster University
Lancaster LA1 4YB (UK)
E-mail: s.sangtarash@lancaster.ac.uk
c.lambert@lancaster.ac.uk
Dr. Ross Davidson
Department of Chemistry, Durham University
Durham, DH1 3LE (UK)
CCDC 1876564 and 1876565 contain the supplementary crystallographic data for this paper. These data are provided free of charge by The Cambridge Crystallographic Data Centre. Further supporting information for this article is given via a link at the end of the document.

investigation of intramolecular QI patterns,[18] combined experimental and theoretical studies of how varying the location and conformation of additional pendant groups can influence through-molecule conductance is lacking. We were therefore motivated to investigate both theoretically and experimentally whether varying the locations and conformations of pendant groups around a molecular backbone could provide a new strategy for tuning QI effects, and hence the molecular conductance.

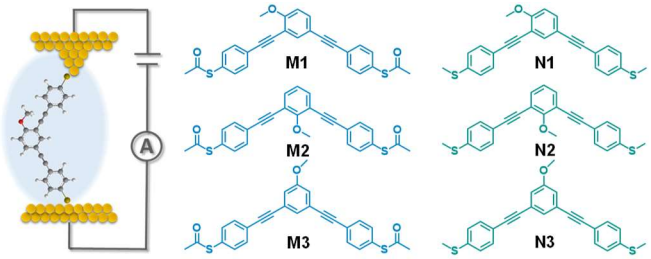

Figure 1. Schematic of STM-BJ setup and the chemical structures of the molecules investigated in this work.

In this study, density functional theory and the scanning tunneling microscope break junction (STM-BJ) technique[19] (Figure 1) are used to investigate single-molecule charge transport through a series of *m*-OPE molecules with thiolate (protected in the precursor as the thioacetyl, SAc) (**M1-3**) or thiomethyl (SMe) (**N1-3**) anchor groups. The synthesis and characterization of all compounds can be found in section S1 of the SI. The two anchor groups are used and results compared to ensure that the phenomena observed are due to the backbone and not some molecule-contact artifacts. The molecular *m*-OPE backbones are systematically modified by introduction of a pendant OMe substituent at different positions around the central ring (Figure 1). The only difference between these molecules is the position and conformation of the pendant OMe group relative to the planar *meta*-diethynylphenylene core. For this molecular system, the OMe pendant groups act as molecular 'taps', which can be used to switch on or off the current flowing through the molecules. Figure 2a shows two conformations of the OMe 'tap' of **N2**. The 'off' conformation (i) features the OMe group perpendicular to the plane of the molecule, and corresponds to a low conductance state for the *m*-OPE fragment, whereas rotating the OMe group into the molecular plane gives the 'on' conformation (ii) and increases molecular conductance through the *m*-OPE moiety. We have designed these molecules, such that the most energetically favorable conformation of the OMe tap belonging to **M1** and **N1** is 'on', whereas that of **M2** and **N2** is 'off'. On the other hand, we have chosen these molecules to demonstrate that the effectiveness of such molecular taps in controlling conductance is critically dependent on their connectivity to the central ring. Therefore we have also chosen the location of the OMe taps of **M3** and **N3** to render them completely ineffective, such that the electrical conductances of **M3** and **N3** are almost independent of the conformation of their pendant OMe groups (Figure S32).

The design of **M1-3** and **N1-3** is informed by the magic ratio theory.[20] This theory describes the effect of connectivity on QI in the central aryl ring, and views the moieties to the left and right as "compound electrodes", which inject and collect electrons via triple bounds into π-orbitals at points *i* and *j* respectively (Figure 2b). The theory applies to the commonly encountered case, where electrons tunnel through the HOMO-LUMO gap (i.e. the Fermi energy of the electrodes lies within the molecular HOMO-LUMO gap). For **M1-3** and **N1-3**, injection and collection points *i* and *j* (Figure 2b) are in *meta* positions relative to each other, and as such the bare 'parent' molecule (with no OMe pendant group) exhibits DQI and possesses a low conductance.[9a] To a first approximation, if a perturbation to the parental structure, due to for example a pendant or substituent group, is imposed on the central ring at a position *k* to yield a 'daughter' molecule, then magic ratio theory predicts the following 'rules'[12]:

1. If, as in **M1** and **N1**, *k* is *ortho* to *i* and *para* to *j*, then the pendant group will increase the conductance by shifting the DQI feature to a higher or lower energy.
2. If, as in **M2** and **N2**, *k* is *ortho* to both *i* and *j*, then the pendant group will increase the conductance by shifting the DQI feature in the opposite direction to case 1.
3. If, as in **M3** and **N3**, *k* is *meta* to either *i* or *j*, then the pendant group will be ineffective and have only a small effect on conductance. Consequently, the conductance of the daughter remains low.

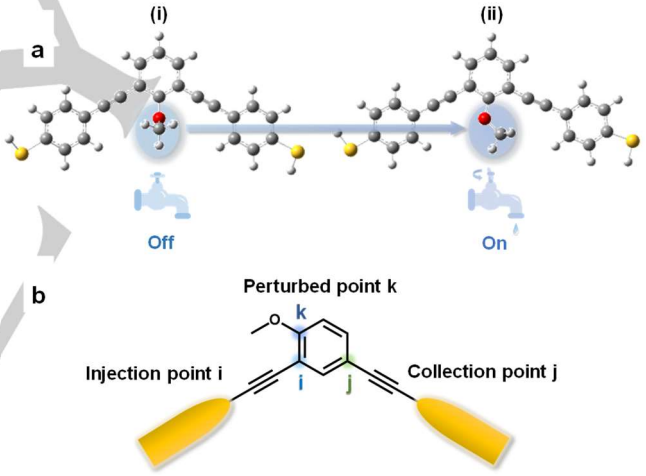

Figure 2. a) Two conformations of the molecular tap M2. Rotating the OMe pendant group from the 'off' conformation (i) to the 'on' conformation (ii) switches the m-OPE molecule from low to high conductance. b) A conceptual view of the magic ratio model of a molecular junction. The yellow regions represent compound electrodes, which inject and collect electrons via triple bonds into π-orbitals of the central ring at points i and j respectively. A perturbation associated with a pendant group is introduced at site k, illustrated schematically here for M1 / N1.

The above changes in conductance are predicted to occur only if the pendant group perturbs the central ring by coupling to its π system (see SI section 6). When this happens, as for the lowest energy conformation of **M1** / **N1** (which also conforms to the crystallographically determined structure of **N1** shown in the SI) or the (higher energy) 'planar' conformation of **M2** / **N2** (c.f. Figure 2a (ii)), we say that the tap is 'on' and the conductances of **M1**, **M2**, **N1** and **N2** will be high. On the other hand, for the most energetically-favourable conformation of **M2** / **N2**, where for steric reasons the OMe group rotates out of the molecular plane ((c.f.

Figure 2a (i)) and the single crystal X-ray structure of **N2** in the SI), the lone pair of electrons on the OMe oxygen atom is orthogonal to the π system of the central ring. In this lower energy 'orthogonal' conformer, the OMe does not significantly perturb the π system of the central ring and the tap is 'off'. Consequently, the conductance of the *m*-OPE daughters **M2 / N2** is expected to remain low. Therefore, by computing and measuring their electrical conductances, we reveal the effect of both connectivity and conformation of the pendant group in controlling the flow of electricity through the *m*-OPE derived molecules.

Results and Discussion

To probe the role of OMe pendant groups, DFT calculations combined with the quantum transport code Gollum[29] were used to compute the transmission coefficient of the systems (see SI section 5). Plots of the transmission coefficients *T(E)* of *m*-OPE **M1-2** and **N1-3** in their fully relaxed geometries are shown in Figure 3a and 3b. The transmission function $T(E_F)$ evaluated at the E_F of the electrodes reflects the magnitude and trends of electrical conductance *G* of the molecules. The experimental location of molecular orbital energies relative to E_F relative may differ from the DFT-predicted values. Typically E_F is expected to lie in the vicinity of the middle of the HOMO-LUMO gap (see supplementary note 9), and based on fitting to the experimentally determined conductance values, our results suggest that E_F falls within the shaded regions in the figure.[30] The resulting theoretical conductances are compared with experimental values in Table 1.

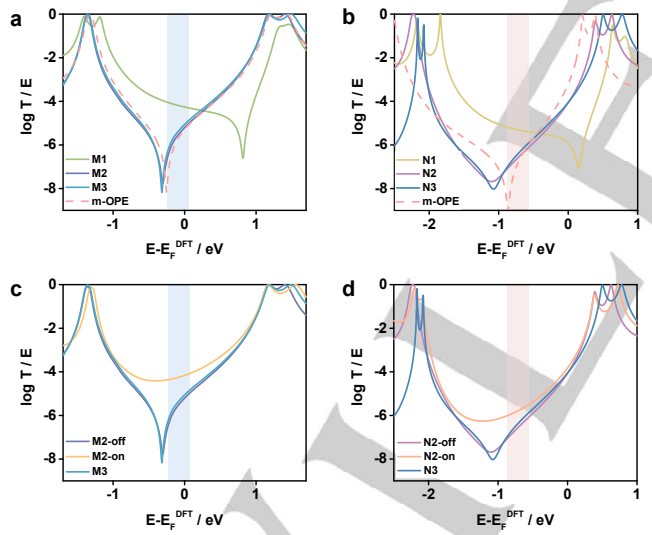

Figure 3. a-b) Transmission coefficients T(E) describing electrons of energy E passing through the m-OPEs from one electrode to the other. In all cases, the dashed lines show results for the parent m-OPE. c-d) Transmission coefficients of the 'off' and 'on' M2 (N2) molecules of Figure 2a (i) and (ii) respectively. For comparison, the conductance of the relaxed M3 (N3) is also shown.

The conductance of thiolate contacted *m*-OPE (i.e. from the SAc protected derivative analogous to the **M**-series of compounds) has been previously determined to be $10^{-5.5}$ G_0.[12b] Figure 3a shows that the transmission function of this parent *m*-OPE (dashed line) possesses a DQI dip near the middle of the HOMO-LUMO gap and that the function is almost coincident with that of **M3** over a wide range of energies, which demonstrates that the OMe tap in this location is ineffective. In contrast, the DQI dip of **M1** is shifted to higher energies and therefore if the Fermi energy E_F in the experiment lies in the vicinity of E_F^{DFT}, the electrical conductance of **M1** is higher than that of **M3** (Figure 3a). These features are also observed in **N1** and **N3** (Figure 3b), and they are in agreement with rules 1 and 3 of the above magic number theory and the trends observed in related studies of the effect of substituent groups on QI.[12, 18b] On the other hand, the DQI dip of **M2** in the fully relaxed geometry is not shifted and therefore the electrical conductance of **M2** remains low. This result for **M2** is entirely consistent with the experimental data presented below (Table 1, Figure 5), but at first inspection would seem to be contrary to the effect of a perturbation described by rule 2, which has been demonstrated to correctly predict the effect of substituents on QI in aryl rings.[12, 18b] However in these earlier studies, molecular conformation plays no role. Here, the transmission coefficients of the 'off' and 'on' conformations of molecules **M2** (Figure 4c) and **N2** (Figure 3d) demonstrate a clear and significant conformational effect. Whilst rotation of the pendant group of **M2** or **N2** into the planar conformation removes the DQI dip from the middle of the HOMO-LUMO gap (Figure 3c, Figure 4d; see also Figure S30), this local minimum described by the planar geometry of the 'on' state is higher than that of the orthogonal conformation (+11.0 (**M2**); +12.7 (**N2**) kJ/mol). Therefore the lower energy 'off' conformations are favoured and determine the conductance properties of the junctions.

Table 1. The calculated and experimentally determined single-molecule conductance of **M1-3** and **N1-3**.

Molecule	Calculated conductance (log(*G*/G_0))	Experimental conductance (log(*G*/G_0))
M1	-4.25	-4.88
M2 (OMe 'on')	-4.18	
M2 (OMe 'off')	-5.24	-5.87
M3	-5.05	-5.55
N1	-5.35	-5.03
N2 (OMe 'on')	-5.557	
N2 (OMe 'off')	-6.26	-5.98
N3	-6.05	-5.74

The presence or absence of DQI transmission dips and the effect on mid-gap conductance can also be linked to the structure of the HOMO and LUMO through a recently highlighted 'orbital product rule' (Figure 4).[31] Even though these molecules do not possess particle-hole symmetry and therefore the orbital-symmetry rule[32] of and the CoulsonRushbrooke pairing theorem [33] do not apply, a qualitative indication of the presence or absence of DQI can be obtained by examining interference between the HOMO and LUMO. The rule is applied by noting that if the HOMO (LUMO) amplitudes of a molecule at the electrode contacts have the same sign, then the HOMO (LUMO) is assigned an "orbital product" a_H (a_L), which is positive. Conversely, if the HOMO (LUMO) amplitudes at the contacts have opposite sign the orbital product a_H (a_L) will be negative. The 'orbital product rule' states that if a_H and a_L possess the same sign (i.e. if the product $a_H \cdot a_L$ is positive) then the HOMO and LUMO interfere destructively and the transmission function is likely to possess a DQI dip, otherwise CQI occurs and there will be no dip. As

indicated in Figure 4, the nodal properties and distribution of the HOMO and LUMO of **N2** in the lower energy 'off' conformation are identical to those of the parent *m*-OPE, because the π system of the pendant OMe group is orthogonal to, and therefore decoupled from, the π system of the central ring. Similar patterns are also found for **N3**, where the OMe pendent is located at a node in both the HOMO and LUMO. In each case, a_H and a_L are both negative, and the orbital product rule predicts that **N2, N3** and the parent *m*-OPE will all exhibit DQI and possess low molecular conductances. In contrast, the opposing signs of a_H and a_L indicate that **N1** should exhibit CQI and possess a high conductance, in agreement with the observed conductance trends (the analogous trends and results from the **M**-series are shown in Table S4). In addition, if the OMe tap of **N2** is artificially rotated to the 'on' position, as shown in the bottom row of Figure 4, the orbital product switches sign and CQI occurs.

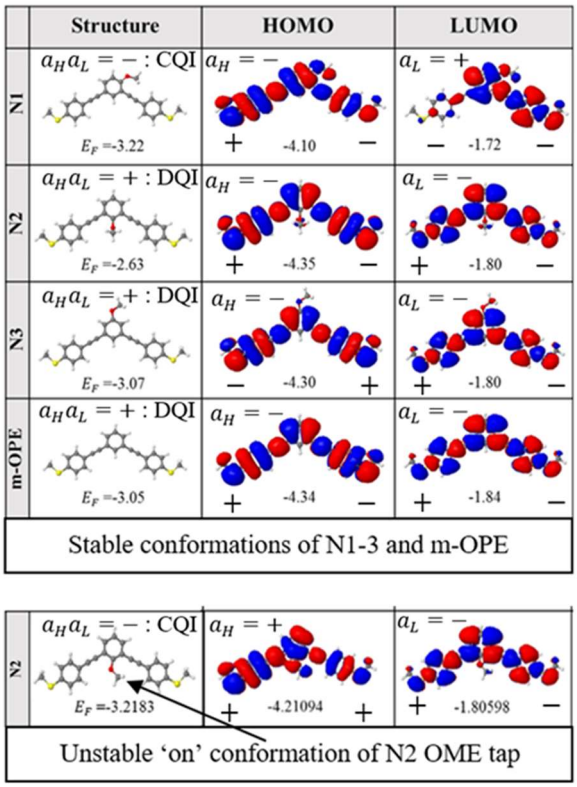

Figure 4. HOMOs and LUMOs of molecules **N1**-**N3** and the parent m-OPE. Blue regions are positive and red regions are negative. As an example, for **N1** the HOMO at the left end of the molecule is positive (+) and at the right end it is negative (-). Therefore, since these have opposite signs, a_H is negative (-). Similarly for **N1**, a_L is negative. Since the product of a_H a_L is positive (+), **N1** will exhibit DQI.

To support the above predictions experimentally, the STM-BJ technique was employed to investigate the single-molecule conductance of all molecules in trimethylbenzene (TMB) at room temperature (see SI section 2 for more details).[21] Typical individual conductance-distance traces of the solvent, **M1-3** and **N1-3** are shown on a semi-logarithmic scale in Figure 5a and 5b.[22] The curves for pure solvent (purple traces) exhibited the expected exponential decay after the cleavage of the last gold-gold atomic contact at the quantum conductance G_0 (G_0 = $2e^2/h$),[23] while the traces for **M1-3** and **N1-3** showed distinct molecular plateaus, indicating the formation of single-molecule junctions. Over 2,000 conductance-distance traces are binned to produce the corresponding 1D histograms featuring distributions with clear peaks (Figure 5c and 5d). These 1D histograms were fitted by Gaussian functions, and the peaks of these distributions are attributed to the conductance of the most probable molecular configurations in the junction i.e. $10^{-4.88}$ G_0, $10^{-5.87}$ G_0 and $10^{-5.55}$ G_0 for **M1-3**, and $10^{-5.03}$ G_0, $10^{-5.98}$ G_0 and $10^{-5.74}$ G_0 for **N1-3**, respectively.

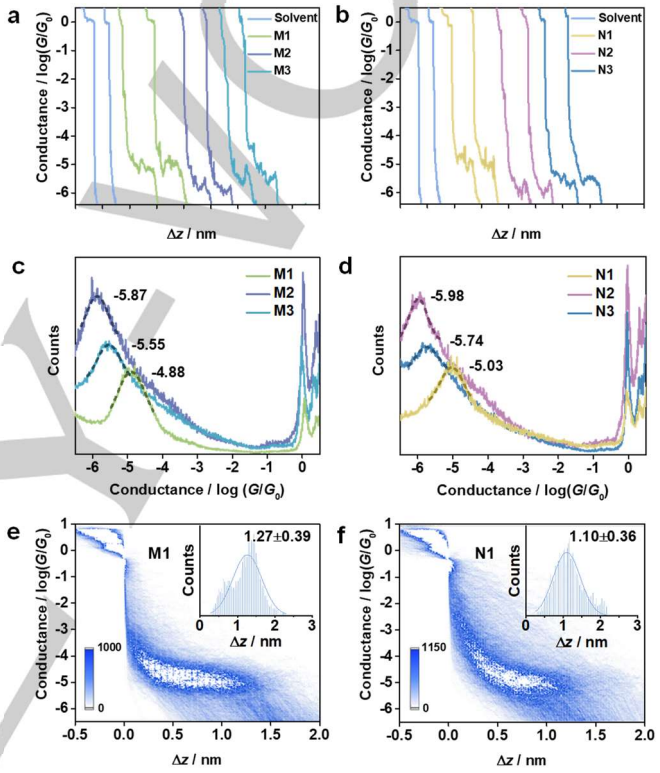

Figure 5. a) Typical individual conductance-distance traces of pure **solvent** (TMB), **M1**, **M2** and **M3**. b) Typical individual conductance-distance traces of pure **solvent** (TMB), **N1**, **N2** and **N3**. c) All-data-point 1D conductance histograms of **M1**, **M2** and **M3** constructed from over 2000 traces for each histogram without data selection. d) All-data-point 1D conductance histograms of **N1**, **N2** and **N3** constructed from over 2000 traces for each histogram without data selection. Representative 2D conductance-displacement histogram and displacement distribution (insertion) of the molecule **M1**. f) Representative 2D conductance-displacement histogram and displacement distribution (insertion) of the molecule **N1**.

The displacement distribution histograms and two-dimensional (2D) conductance-displacement histograms of **M1** and **N1** are shown in Figure 5e and 5f by way of example (for the analogous data from the other molecules see Figure S25.[24] In the case of **M1** by way of example, the most probable length of the molecular junction is determined to be 1.77±0.39 nm after correcting for the snap-back effect of the gold-gold atomic contact (0.5 nm) (Figure 5e, S3).[21] These measurements and computational estimates of the junction length are remarkably consistent with all the members of both series (Figure S25, Table S1 and S3), suggesting that the molecules are contacted through the sulfur atoms in the molecular

junctions. The **M2**/**N2** and **M3**/**N3** seem to express the broader conductance features than **M1**/**N1**. This is because the conductances of **M2**/**N2** and **M3**/**N3** are very close to the lower detection limit of our instrument (-7 ~ -6.5 log (G / G_0)) and the external electromagnetic interference and mechanical vibration will have more obvious influence on these conductance data. In order to avoid the influence of the unstable molecular junctions on the measurements, we reconstruct 1D conductance histograms by collecting data points within the limited displacement range (0.9 ~ 1.1 nm) where the conductance plateaus are relatively flat and close to full extension (See Figure S31 for more details). The conductance peaks display that the conductance values are very similar to the results of the original full-range 1D conductance histograms, suggesting that the unstable junctions or lower yields of junctions might affect the shapes and distributions of 1D conductance histograms but not distinctly change the conductance values.

To exclude the influence of physisorbed sulphur contacts and formation of junctions retaining the acetyl-protecting groups,[25] single-molecule measurements of the **M**-series of molecules were also recorded after adding 3 equiv. of Bu_4NOH to the sample solution to ensure cleavage of the acetyl moiety. The resulting conductance-distance traces and conductance histograms were consistent with those of the same molecules measured in pristine solvent (Figure S27-S29).[25-26] To rule out the further possibilities of intramolecular π-π stacking effects within the junction[27] or adventitious electrode contacts to the methoxy moiety[28], two model tolane compounds (4-((4-methoxyphenyl)ethynyl)phenyl) (methyl)sulfane **(O1**) and (4-((3-methoxyphenyl)ethynyl)phenyl) (methyl)sulfane (**O2**) were also measured (Figure S26). Under conditions identical to those used in the studies of **M1-3** and **N1-3**, no clear molecular plateaus were observed in the conductance histograms of **O1** and **O2**. These control experiments, together with the excellent agreement of the break-off distance and the molecular length of **M1-3** and **N1-3** give us confidence that the single-molecule conductance features illustrated in Figure 5 can be attributed to single-molecule junctions formed by contact of the gold electrodes to the two sulfur atom anchors of **M1-3** and **N1-3**.

The conductance values (*G*) within each series follow a pronounced pattern of variation, with *G* (**M1 / N1**) > *G* (**M3 / N3**) > *G* (**M2** / **N2**). This pattern of behaviour is entirely consistent with the broad predictions of the magic ratio theory described above, combined with the DFT predictions for the conformation of the OMe pendant relative to the central phenylene ring, which determines the on-off nature of the OMe 'tap'.

Conclusion

In conclusion, we have investigated the possibility of tuning DQI within *m*-OPE derived molecules by placing OMe pendant 'taps' at different positions around the central ring. Our combined DFT predictions and MJBJ measurements demonstrate that the position and orientation of the OMe taps have a significant impact on the energy of the DQI induced dips in the transmission function. As a consequence of this DQI tuning, the conductance of **M1/N1** is almost one order of magnitude higher than the parent *m*-OPE system**,** whereas the conductances of **M3/N3** remain low. On the other hand, the influence of the OMe group on the mid-gap DQI feature also strongly depends on the on-off conformation of the OMe tap. This is illustrated by **M2/N2,** whose most energetically favourable conformation is 'off' and corresponds to weak coupling between the pendant group and the molecular core. This work presents a simple and convenient approach for structurally tuning room-temperature DQI at a single-molecule level and demonstrates a new strategy for designing molecular devices with enhanced switching functionality.

Experimental Section

Synthesis: The target compounds **M1-3** were prepared by Sonogashira cross-coupling of an appropriate isomer of 1,3-diethynyl anisole with *S*-4-iodophenyl ethanethioate. Compound **N1** was prepared in an analogous fashion from 1,3-diethynyl-4-methoxybenzene and (4-iodophenyl)(methyl)sulfane, whilst it proved more convenient to prepare **N2** and **N3** from (4-ethynylphenyl)(methyl)sulfane and the appropriate 1,3-diiodo or 1,3-dibromo anisole as detailed in the supporting information (see SI section 1).

Conductance measurements: Conductance measurements were made using the STM-BJ technique to form gold-molecule-gold junctions from 0.1 mM solutions of the target compound in 1,3,5-trimethylbenzene (TMB, 99%, Sigma-Aldrich used as received). Gold wire (99.99%, 0.25mm diameter) was purchased from Beijing Jiaming Platinum Nonferrous Metal Co, Ltd. for the fabrication of STM tip. A polytef liquid cell and a perfluoroelastomer O-ring (FFKM 6.07 × 1.78) were purchased from Wuxi Bo Yate Sealing Technology Development Co. Ltd. All measurements were carried out at room temperature. Substrates were prepared by depositing gold film on the N<111> monocrystalline face of a silicon wafer. The gold-coated substrate were cleaned by immersion in piranha solution (V (H_2SO_4): V(H_2O_2) = 3:1 CAUTION piranha solution is extremely corrosive) for ca. 2 hours, before being rinsed three times in fresh, boiling deionized water for 5-15 minutes. After this time the substrate was moved into fresh deionised water and the boiling procedure repeated for a total of three cycles. The polytef liquid cell and a perfluoroelastomer O-ring were also be cleaned in a similar fashion before being clamped to the substrate to create the liquid cell. The gold wire was carefully cleaned and annealed in a butane flame before use. After measurement, 1D conductance histograms were used to determine the most likely conductance values, whilst 2D conductance-displacement cloud maps provided additional information of the stretching distance for the molecular plateaus. Further information can be found in SI section 2.

Theoretical methods: The optimized geometry and ground state Hamiltonian and overlap matrix elements of each structure were self-consistently obtained using the SIESTA implementation of density functional theory (DFT). SIESTA employed norm-conserving pseudo-potentials to account for the core electrons and linear combinations of atomic orbitals to construct the valence states. The generalized gradient approximation (GGA) of the exchange and correlation functional was used with the Perdew-Burke-Ernzerhof parameterization (PBE), a double-ζ polarized (DZP) basis set, a real-space grid defined with an equivalent energy cut-off of 250 Ry. The geometry optimization for each structure was performed to the forces smaller than 10 meV/Ang. The mean-field Hamiltonian obtained from the converged DFT calculation or a simple tight-binding Hamiltonian was combined

with our Gollum quantum transport code to calculate the phase-coherent, elastic scattering properties of the each system consist of left (source) and right (drain) leads and the scattering region. The transmission coefficient T (E) for electrons of energy E (passing from the source to the drain) was calculated via the relation $T(E) = Trace(\Gamma_R(E)G^R(E)\Gamma_L(E)G^{R\dagger}(E))$. In this expression, $\Gamma_{L,R}(E) = i\left(\sum_{L,R}(E) - \sum_{L,R}{}^{\dagger}(E)\right)$ described the level broadening due to the coupling between left (L) and right (R) electrodes and the central scattering region, $\sum_{L,R}(E)$ were the retarded self-energies associated with this coupling and $G^R = (ES - H - \sum_L - \sum_R)^{-1}$ was the retarded Green's function, where H was the Hamiltonian and S was overlap matrix. Using obtained transmission coefficient ($T(\mathrm{E})$), the conductance could be calculated by Landauer formula ($\mathrm{G} = \mathrm{G}_0 \int \mathrm{dE}\, \mathrm{T}(\mathrm{E})(-\partial \mathrm{f}/\partial \mathrm{E})$) where $G_0 = 2e^2/h$ was the conductance quantum, $f(E) = (1 + exp((E - E_F)/k_BT))^{-1}$ was the Fermi-Dirac distribution function, T was the temperature and k_B = 8.6×10^{-5} eV/K was Boltzmann's constant.

Acknowledgments

This work was supported by the National Key R&D Program of China (2017YFA0204902), National Natural Science Foundation of China (Nos. 21673195, 21703188, 21503179). It was also supported by EPSRC grants EP/P027156/1, EP/N03337X/1, EP/N017188/1, the EC H2020 FET Open project 767187 "QuIET", the EU project Bac-to-Fuel and the Australian Research Council (DP190100074). S.S. acknowledge the Leverhulme Trust (Leverhulme Early Career Fellowships no. ECF-2018-375) for funding. H.S. acknowledges the UKRI Future Leaders Fellowship no. MR/S015329/1. M. N. and M. K. gratefully acknowledge support from the Forrest Research Foundation. The crystallographic structures of N1 and N2 were determined using facilities and instrumentation provided by the Centre for Microscopy, Characterisation and Analysis (CMCA), University of Western Australia.

Keywords: density functional calculations • destructive quantum interference • scanning tunnelling microscope break junction • single-molecule studies

[1] a) N. Algethami, H. Sadeghi, S. Sangtarash, C. J. Lambert, *Nano Lett.* **2018**, *18*, 4482-4486; b) W. Xu, E. Leary, S. Hou, S. Sangtarash, M. T. González, G. Rubio-Bollinger, Q. Wu, H. Sadeghi, L. Tejerina, K. E. Christensen, N. Agraït, S. J. Higgins, C. J. Lambert, R. J. Nichols, H. L. Anderson, *Angew. Chem. Int. Ed.* **2019**, *58*, 8378-8382.

[2] a) C. D. Frisbie, *Science* **2016**, *352*, 1394-1395; b) F. Chen, J. He, C. Nuckolls, T. Roberts, J. E. Klare, S. Lindsay, *Nano Lett.* **2005**, *5*, 503-506; c) T. A. Su, H. Li, M. L. Steigerwald, L. Venkataraman, C. Nuckolls, *Nat. Chem.* **2015**, *7*, 215-220.

[3] a) X. Chen, M. Roemer, Y. Li, D. Wei, D. Thompson, E. D. Barco, C. A. Nijhuis, *Nat. Nanotechnol.* **2017**, *12*, 797-803; b) I. Díez-Pérez, J. Hihath, Y. Lee, L. Yu, L. Adamska, M. A. Kozhushner, I. I. Oleynik, N. Tao, *Nat. Chem.* **2009**, *1*, 635-641.

[4] a) M. H. Garner, H. Li, Y. Chen, T. A. Su, Z. Shangguan, D. W. Paley, T. Liu, F. Ng, H. Li, S. Xiao, C. Nuckolls, L. Venkataraman, G. C. Solomon, *Nature* **2018**, *558*, 415-419; b) R. Frisenda, V. A. E. C. Janssen, F. C. Grozema, H. S. J. van der Zant, N. Renaud, *Nat. Chem.* **2016**, *8*, 1099-1104.

[5] G. I. Taylor, Proc. Camb. Phil. Soc. 15, 114-115 (1909).

[6] a) N. C. Harris, G. R. Steinbrecher, M. Prabhu, Y. Lahini, J. Mower, D. Bunandar, C. Chen, F. N. C. Wong, T. Baehr-Jones, M. Hochberg, S. Lloyd, D. Englund, *Nature Photon.* **2017**, *11*, 447-453; b) A. Sipahigil, R. E. Evans, D. D. Sukachev, M. J. Burek, J. Borregaard, M. K. Bhaskar, C. T. Nguyen, J. L. Pacheco, H. A. Atikian, C. Meuwly, R. M. Camacho, F. Jelezko, E. Bielejec, H. Park, M. Lončar, M. D. Lukin, *Science* **2016**, *354*, 847-850.

[7] a) C. Schuck, X. Guo, L. Fan, X. Ma, M. Poot, H. X. Tang, *Nat.Commun.* **2016**, *7*, 10352; b) S. Goswami, E. Mulazimoglu, A. M. R. V. L. Monteiro, R. Wölbing, D. Koelle, R. Kleiner, Y. M. Blanter, L. M. K. Vandersypen, A. D. Caviglia, *Nat. Nanotechnol.* **2016**, *11*, 861-865.

[8] Z.-E. Su, Y. Li, P. P. Rohde, H.-L. Huang, X.-L. Wang, L. Li, N.-L. Liu, J. P. Dowling, C.-Y. Lu, J.-W. Pan, *Phys. Rev. lett.* **2017**, *119*, 080502.

[9] a) C. Lambert, *Chem. Soc. Rev.* **2015**, *44*, 875-888; b) D. Xiang, X. Wang, C. Jia, T. Lee, X. Guo, *Chem. Rev.* **2016**, *116*, 4318-4440.

[10] Y. Zhang, G. Ye, S. Soni, X. Qiu, T. L. Krijger, H. T. Jonkman, M. Carlotti, E. Sauter, M. Zharnikov, R. C. Chiechi, *Chem. Sci.* **2018**, *9*, 4414-4423.

[11] M. Kiguchi, T. Ohto, S. Fujii, K. Sugiyasu, S. Nakajima, M. Takeuchi, H. Nakamura, *J. Am. Chem. Soc.* **2014**, *136*, 7327-7332.

[12] a) S. Sangtarash, H. Sadeghi, C. J. Lambert, *Phys. Chem. Chem. Phys.* **2018**, *20*, 9630-9637; b) X. Liu, S. Sangtarash, D. Reber, D. Zhang, H. Sadeghi, J. Shi, Z. Y. Xiao, W. Hong, C. J. Lambert, S. X. Liu, *Angew. Chem. Int. Ed.* **2017**, *56*, 173-176.

[13] X. F. Li, Q. Qiu, Y. Luo, *J. Appl. Phys.* **2014**, *116*, 013701.

[14] C. M. Guédon, H. Valkenier, T. Markussen, K. S. Thygesen, J. C. Hummelen, S. J. Van Der Molen, *Nat. Nanotechnol.* **2012**, *7*, 305-309.

[15] C. R. Arroyo, S. Tarkuc, R. Frisenda, J. S. Seldenthuis, C. H. Woerde, R. Eelkema, F. C. Grozema, H. S. Van Der Zant, *Angew. Chem. Int. Ed.* **2013**, *52*, 3152-3155.

[16] D. Z. Manrique, C. Huang, M. Baghernejad, X. Zhao, O. A. Al-Owaedi, H. Sadeghi, V. Kaliginedi, W. Hong, M. Gulcur, T. Wandlowski, *Nat. Commun.* **2015**, *6*, 6389; D.Zsolt Manrique, Q. Al-Galiby, W. Hong, and C. J. Lambert, Nano Letters 16, 1308−1316 (2016).

[17] a) Y. Li, M. Buerkle, G. Li, A. Rostamian, H. Wang, Z. Wang, D. R. Bowler, T. Miyazaki, L. Xiang, Y. Asai, G. Zhou, N. Tao, *Nat. Mater.* **2019**, *18*, 357-363; b) J. Bai, A. Daaoub, S. Sangtarash, X. Li, Y. Tang, Q. Zou, H. Sadeghi, S. Liu, X. Huang, Z. Tan, J. Liu, Y. Yang, J. Shi, G. Mészáros, W. Chen, C. Lambert, W. Hong, *Nat. Mater.* **2019**, *18*, 364-369.

[18] a) A. Danilov, S. Kubatkin, S. Kafanov, P. Hedegård, N. Stuhrhansen, K. Mothpoulsen, T. Bjørnholm, *Nano Lett.* **2008**, *8*, 1-5; b) M. H. Garner, G. C. Solomon, M. Strange, *J. Phys. Chem.C* **2016**, *120*, 9097-9103; c) G. C. Solomon, D. Q. Andrews, R. H. Goldsmith, T. Hansen, M. R. Wasielewski, R. P. Van Duyne, M. A. Ratner, *J. Am. Chem. Soc.* **2008**, *130*, 17301-17308.

[19] B. Xu, N. J. Tao, *Science* **2003**, *301*, 1221-1223.

[20] S. Sangtarash, H. Sadeghi, C. J. Lambert, *Nanoscale* **2016**, *8*, 13199.

[21] W. Hong, H. Valkenier, G. Mészáros, D. Z. Manrique, A. Mishchenko, A. Putz, P. M. García, C. J. Lambert, J. C. Hummelen, Wandlowski, Thomas, *Beilstein J. Nanotechnol.* **2011**, *2*, 699-713.

[22] W. Hong, D. Z. Manrique, P. Moreno-García, M. Gulcur, A. Mishchenko, C. J. Lambert, M. R. Bryce, T. Wandlowski, *J. Am. Chem. Soc.* **2012**, *134*, 2292-2304.

[23] R. Huber, M. T. González, S. Wu, M. Langer, S. Grunder, V. Horhoiu, M. Mayor, M. R. Bryce, C. Wang, R. Jitchati, C. Schönenberger, M. Calame, *J. Am. Chem. Soc.* **2008**, *130*, 1080-1084.

[24] D. Z. Manrique, C. Huang, M. Baghernejad, X. Zhao, O. A. Al-Owaedi, H. Sadeghi, V. Kaliginedi, W. Hong, M. Gulcur, T. Wandlowski, M. R. Bryce, C. J. Lambert, *Nat. Commun.* **2015**, *6*, 6389.

[25] M. T. GonzáLez, E. Leary, R. Garcia, P. Verma, M. A. N. Herranz, G. Rubio-Bollinger, N. Martin, N. Agrait, *J. Phys. Chem. C* **2011**, *115*, 17973-17978.

[26] V. Hennie, E. H. Huisman, P. A. Hal, Van, D. M. Leeuw, De, R. C. Chiechi, J. C. Hummelen, *J. Am. Chem. Soc.* **2011**, *133*, 4930-4939.

[27] S. Martín, I. Grace, M. R. Bryce, C. Wang, R. Jitchati, A. S. Batsanov, S. J. Higgins, C. J. Lambert, R. J. Nichols, *J. Am. Chem. Soc.* **2010**, *132*, 9157-9164.

[28] O. A. Al-Owaedi, S. Bock, D. C. Milan, M.-C. Oerthel, M. S. Inkpen, D. S. Yufit, A. N. Sobolev, N. J. Long, T. Albrecht, S. J. Higgins, *Nanoscale* **2017**, *9*, 9902-9912.

[29] J. Ferrer, C. J. Lambert, V. M. García-Suárez, D. Z. Manrique, D. Visontai, L. Oroszlany, R. Rodríguez-Ferradás, I. Grace, S. Bailey, K. Gillemot, *New J. Phys.* **2014**, *16*, 093029.

[30] a) H. Song, Y. Kim, Y. H. Jang, H. Jeong, M. A. Reed, T. Lee, *Nature* **2009**, *462*, 1039-1043; b) P. Moreno-García, M. Gulcur, D. Z. Manrique, T. Pope, W. Hong, V. Kaliginedi, C. Huang, A. S. Batsanov, M. R. Bryce, C. Lambert, *J. Am. Chem. Soc.* **2013**, *135*, 12228-12240.

[31] C. J. Lambert, S. X. Liu, *Chem.–A Eur. J.* **2018**, *24*, 4193-4201.

[32] K.Yoshizawa, T. Tada, and A. Staykov, J. Am. Chem. Soc. 130, 9406 (2008); X. Li, A. Staykov, and K. Yoshizawa, J. Phys. Chem. C 114, 9997 (2010); Y. Tsuji, A. Staykov, and K. Yoshizawa, J. Am. Chem. Soc. 133, 5955 (2011)

[33] C. A. Coulson and G. S. Rushbrooke, Math. Proc. Cambridge Philos. Soc. 36, 193 (1940)

RESEARCH ARTICLE

The change of the conformation and location of an –OMe group at different positions can serve as a ‘molecular tap’, which will precisely control the ‘on-off’ state of the m-OPE in their electrical conductance and offer a convenient and simple way to control room-temperature charge transport at the single-molecule scale.

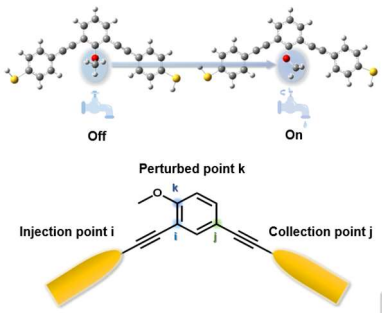

Feng Jiang, Douglas I. Trupp, Norah Algethami, Haining Zheng, Wenxiang He, Afaf Alqorashi, Chenxu Zhu, Chun Tang, Ruihao Li, Junyang Liu, Hatef Sadeghi, Jia Shi, Ross Davidson, Marcus Korb, Alexandre N. Sobolev, Masnun Naher, Sara Sangtarash, Paul J. Low,* Wenjing Hong,* Colin J. Lambert**

Page No. – Page No.

Turning the Tap: Conformational Control of Quantum Interference to Modulate Single Molecule Conductance